Available online at www.sciencedirect.com
ScienceDirect
European Journal of Mechanics B/Fluids 26 (2007) 738–748

Particle tracking in Taylor–Couette flow

Karen L. Henderson [a,*], D. Rhys Gwynllyw [a], Carlo F. Barenghi [b]

[a] *School of Mathematical Sciences, University of the West of England, Bristol, BS16 1QY, UK*
[b] *School of Mathematics and Statistics, University of Newcastle, Newcastle upon Tyne, NE1 7RU, UK*

Received 28 June 2006; received in revised form 13 December 2006; accepted 21 December 2006

Available online 11 January 2007

Abstract

The paths of small inertial particles are computed in a steady Taylor vortex background flow. When buoyancy effects are neglected we find that particles denser than the background fluid tend to a limit orbit in the meridional plane. The difference in settling time and orbit size, with varying Reynolds number of the background flow, is investigated. We also consider the effect of the various forces on the limit orbit of the particle.

Keywords: Taylor–Couette flow; Inertial particles; Settling behaviour

1. Introduction

We track the motion of small inertial spherical particles in steady, axisymmetric Taylor vortex flow using the Maxey and Riley equations [1] with the corrected form for the added mass force, as detailed by Auton et al. [2]. These equations were written in the correct form by Mei [3]. This work is motivated firstly by recent experimental techniques [4–6] which have enabled Particle Image Velocimetry (PIV) experiments to be carried out in helium II. Couette flow is a well-known benchmark of superfluid hydrodynamics [7] and the possibility of using tracer particles to visualise the motion of helium II is an exciting development. Secondly, the Couette apparatus has been used as a rotating filter for many years as a means, for example, of separating plasma from blood. More recently there has been interest in further uses of the Couette system, for example as a photocatalytic reactor for water purification [8] and as a bioreactor for the culture of animal cells [9]. Thirdly, there has been renewed interest in the equations of the particle motion; Babiano et al. [10] have found that neutrally buoyant particles separate from fluid trajectories in regions where the flow has hyperbolic stagnation points.

There is a vast literature on particle tracking using variations of the particle tracking equations in different geometries, see Michaelides [11] for an overview. The motion of particles in the Taylor–Couette geometry has also been covered widely, due to its use as a rotating filtration device [12–14]. However, much of this research has concentrated on the filtration performance in specific applications as opposed to considering the individual particle motion.

* Corresponding author.
E-mail addresses: karen.henderson@uwe.ac.uk (K.L. Henderson), rhys.gwynllyw@uwe.ac.uk (D.R. Gwynllyw), c.f.barenghi@ncl.ac.uk (C.F. Barenghi).

0997-7546/$ – see front matter
doi:10.1016/j.euromechflu.2006.12.001

In Taylor vortex flow the motion of individual particles has been investigated in detail by only two research groups. Rudman [15,16] tracked inertial particles in both wavy and non-wavy vortex flow fields. Their primary interest was the strain history that inertial particles experienced due to their paths and the dispersion of fluid particles. Wereley and Lueptow [17] used an analytic representation of Taylor–Couette flow obtained by a weakly non-linear amplitude approach [18] to model the background flow. This approach is only valid at Reynolds numbers just a few percent above the critical value at which Couette flow becomes unstable. They focused their research on the segregation of the particles due to interaction with Taylor vortices. Various particle densities were considered and a net radial flow was imposed. Both groups neglected some of the forces acting on the particle. One aim of this paper is to investigate the effect the individual forces acting on the particle have on its subsequent motion, in order to see whether their neglection is justified in subsequent studies. A second aim of the paper is to investigate how varying the Reynolds number affects the particle motion. For the background flow we use a numerical solution to the Navier–Stokes equations, which is valid for Reynolds numbers up to the point at which wavy modes appear, so we are able to explore a wider range of Reynolds numbers than Wereley and Lueptow [17].

The structure of the paper is as follows; in Section 2 we discuss how the background flow is computed and how we track the particles in this flow. In Section 3 we display the results of tracking particles in a Taylor vortex flow, plotting individual particle paths and considering the effects of neglecting some of the forces acting on the particle. Finally, in Section 4 we discuss the implications of these results.

2. Model

2.1. Background flow

We consider a classical Navier–Stokes fluid to be contained between two vertical concentric cylinders of inner radius R_1 and outer radius R_2. The outer cylinder is held fixed and the inner cylinder rotates at constant angular velocity Ω_1. We make the usual simplifying assumption that the cylinders have infinite length and compute the steady axisymmetric Taylor vortex flow using a spectral code [19]. Once the spectral coefficients of the background flow have been found, the fields required to calculate the forces acting on the particles may be evaluated at any point in the annulus. For example, the azimuthal component of velocity of the background flow, $(\boldsymbol{v}_f)_\phi$ at position (r, z) is given by

$$(\boldsymbol{v}_f)_\phi = \sum_{m=1}^{M+1} \sum_{k=1}^{K} v_{mk} \cos\big[(m-1)\alpha z\big] T^*_{k-1}(r - R_1) \tag{1}$$

where v_{mk} are the spectral coefficients, T^*_k is the Chebychev polynomial of the first kind and M, K are the discretisation parameters.

The controlling parameters of this background flow are the Reynolds number of the inner cylinder $Re = \Omega_1 R_1 \delta/\nu$ and the radius ratio $\eta = R_1/R_2$, where $\delta = R_2 - R_1$ is the gap between the cylinders and ν is the kinematic viscosity of the fluid. A schematic diagram of the background flow is shown in Fig. 1. For a given value of η, the axial wavenumber,

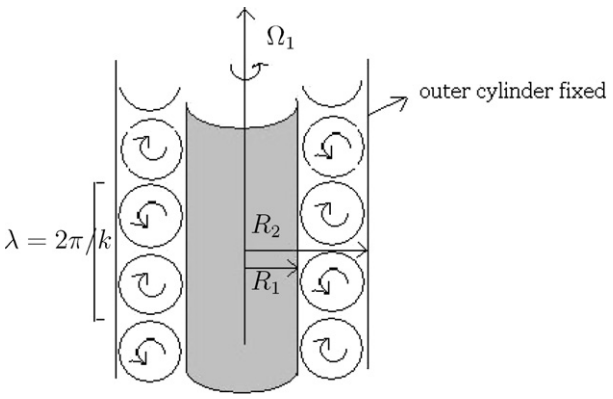

Fig. 1. A schematic of the background flow.

k, of the flow, which determines the wavelength $\lambda = 2\pi/k$ of a pair of Taylor cells, is taken to be the critical value for which Couette flow becomes linearly unstable. Throughout this paper, we consider a radius ratio of $\eta = 0.75$. This enables us to explore a large range of Reynolds numbers in the Taylor vortex regime.

2.2. Particle tracking

We model the motion of rigid spherical particles of radius a_p in the background flow, detailed in Section 2.1. We assume that the particles do not affect the background flow and do not interact with each other. Provided that the particle Reynolds number based on the relative velocity is small, $Re_t \equiv 2a_p|\boldsymbol{u}_p - \boldsymbol{v}_f|/\nu \ll 1$, the equations may be expressed as

$$\begin{aligned} m_p \frac{\mathrm{d}\boldsymbol{u}_p}{\mathrm{d}t} = {} & m_f \frac{D\boldsymbol{v}_f}{Dt} - \frac{1}{2} m_f \left\{ \frac{\mathrm{d}\boldsymbol{u}_p}{\mathrm{d}t} - \frac{D}{Dt}\left(\boldsymbol{v}_f + \frac{1}{10} a_p^2 \nabla^2 \boldsymbol{v}_f \right) \right\} + (m_p - m_f)\boldsymbol{g} \\ & - 6\pi a_p \nu \rho_f \int_0^t K(t-\tau,\tau) \frac{\mathrm{d}}{\mathrm{d}\tau}\left(\boldsymbol{u}_p - \boldsymbol{v}_f - \frac{1}{6} a_p^2 \nabla^2 \boldsymbol{v}_f \right) \mathrm{d}\tau \\ & - 6\pi a_p \nu \rho_f \left(\boldsymbol{u}_p - \boldsymbol{v}_f - \frac{1}{6} a_p^2 \nabla^2 \boldsymbol{v}_f \right) + 6.46 a_p^2 \rho_f \sqrt{\frac{\nu}{|\boldsymbol{\omega}_f|}} (\boldsymbol{v}_f - \boldsymbol{u}_p) \times \boldsymbol{\omega}_f = \boldsymbol{F} \end{aligned} \tag{2}$$

where m_p is the mass of the particle, m_f is the mass of the fluid displaced by the particle, ρ_f is the density of the background fluid, $\boldsymbol{u}_p$ is the velocity of the particle, $\boldsymbol{\omega}_f = \operatorname{curl} \boldsymbol{v}_f$ is the vorticity of the background flow and $\boldsymbol{g}$ is the acceleration due to gravity. The terms $\mathrm{d}/\mathrm{d}t$ and D/Dt represent the Lagrangian derivatives following the particle and fluid respectively. The terms on the right-hand side represent the inertial force, the added mass force, the buoyancy term, the Basset [20] history force, the Stokes drag force and the Saffman shear-induced lift force, respectively. The three terms involving $\nabla^2 \boldsymbol{v}_f$ are the Faxén corrections and take into account the curvature in the velocity field of the fluid. In computing the Basset history force we assume that the initial velocity of the particle is equal to that of the fluid, at the initial position of the particle, and use the kernel $K(t, t-\tau)$ as proposed by Mei and Adrian [21], that is

$$K(t-\tau,\tau) = \left\{ \left[\frac{\pi(t-\tau)\rho_f \nu}{a_p^2} \right]^{1/4} + \left[\frac{\pi}{2} \frac{|\boldsymbol{v}_f - \boldsymbol{u}_p|^3}{a_p \rho_f \nu f_H^3(Re_t)} (t-\tau)^2 \right]^{1/2} \right\}^{-2} \tag{3}$$

where $f_H(Re_t) = 0.75 + 0.105 Re_t(\tau)$. This kernel decays as $(t-\tau)^{-1/2}$ in the short term and as $(t-\tau)^{-2}$ in the long term as required. The centrifugal and Coriolis accelerations acting on the particle do not appear explicitly in Eq. (2) but appear implicitly in the terms containing the particle velocity, when properly accounting for the rotating frame of reference.

Eq. (2) may be rearranged into the form

$$m_0 \frac{\mathrm{d}\boldsymbol{u}_p}{\mathrm{d}t} = \boldsymbol{f} \tag{4}$$

where $m_0 = m_p + m_f/2$ and $\boldsymbol{f} = \boldsymbol{F} + \frac{1}{2} m_f \, \mathrm{d}\boldsymbol{u}_p/\mathrm{d}t$. This equation needs to be solved together with the differential equation

$$\frac{\mathrm{d}\boldsymbol{r}_p}{\mathrm{d}t} = \boldsymbol{u}_p \tag{5}$$

where $\boldsymbol{r}_p$ is the position of the particle at time t. Eqs. (4), (5) are solved numerically using an implicit two-stage Runge–Kutta scheme with fixed point iteration. For the results presented we have checked that the particle Reynolds number, Re_t, remains small throughout the calculation. All the results in this paper are presented to graphical tolerance.

In tracking the motion of particles, researchers often neglect some of the forces detailed in Eq. (2). In Taylor–Couette flow, Wereley and Lueptow [17] neglected the Basset and Saffman forces and used a different form for the added mass force. The Faxén corrections were included and for neutrally buoyant particles a slight deviation of the particle paths from fluid element paths was noted as a result. Rudman [15] neglected the Basset, Faxén and Saffman forces.

The Basset force is expensive to compute as it involves a summation at each time-step. The computation can be simplified somewhat by transforming Eq. (2) to a second order differential equation in the relative velocity $\boldsymbol{u}_p - \boldsymbol{v}_f$ [22].

This simplification approach is not necessary for the current work because we are tracking only a few particles. There have been several studies looking at the effects and relative importance of this term, but none in the Couette geometry. Candelier et al. [23] investigated its effect on the radial migration of a Stokes particle in a vortex. They found that the relative difference between including and neglecting the history force on the ejection rate of the particle scaled as the square root of the Stokes number, *St* (the ratio of the particle viscous response time to the characteristic time of the background flow) so the history force can have an appreciable effect even at small values of *St*. Other studies of the effect of the Basset force have been performed [11,24,25]. The Saffman lift force is typically neglected when the particle Reynolds number is small. We anticipate that in Taylor vortex flow it may have an appreciable effect when the particle is near the inner cylinder, where the shear is large. Coimbra and Kobayashi [26] considered the viscous motion of a small particle in a rotating cylinder and found quite different results when comparing them with and without the lift force. For small particles, the Faxén terms will become significant only if the curvature of the background velocity profile becomes large. This is unlikely to be the case for Taylor vortex flow so we do not expect to see a qualitative difference from including these corrections.

One of the aims of this paper is to investigate the effect that each of the forces has on the subsequent motion of the particles. It is clear that including the buoyancy term may have a significant effect on the particle paths of non-neutrally buoyant particles, transporting particles from one Taylor cell to another [17,27]. This term may be neglected when the sedimentation velocity,

$$u_\infty = \frac{2a_p^2 g(\rho_p - \rho_f)}{9\rho_f \nu},$$

taken to be the terminal velocity of a particle placed in a stationary background flow, is small compared to the characteristic velocities of the fluid. For completeness, we have included the buoyancy term in Eq. (2), however in this paper we want to investigate in particular the effects of the Basset, Faxén and Saffman forces on the particle. Therefore we choose to set the buoyancy term to zero, in order to isolate these effects to one Taylor cell.

3. Results

Particles can be characterised by two parameters, density ratio $\beta = \rho_p/\rho_f$ and particle ratio $\alpha_p = \delta/2a_p$, where ρ_p represents the density of the particle. Results presented in this section are for a particle with $\beta = 1.05$, $\alpha_p = 29.6$ unless stated otherwise. In Figs. 5, 8 we investigate the effect of changing these particle parameters. In Section 3.1 we illustrate the motion of particles in a Taylor–Couette flow for different initial positions and at varying Reynolds numbers. The results in this section are produced neglecting the Basset force, Faxén corrections and Saffman force. In Section 3.2 we investigate the effect of including these three forces on the subsequent motion of the particle.

3.1. Motion of particles

In Fig. 2(a) we plot the projection in a meridional plane of the paths of two particles ($\beta = 11$) in a single clockwise Taylor vortex in a flow with Reynolds number $Re = 120$. The particle paths can be considered to be a superposition of azimuthal motion around the inner cylinder and toroidal motion in the vertical plane. As reported by Wereley and Lueptow [17] we find that the particles tend to a limit cycle orbit in a meridional plane. That is, a particle that is initially close to the edge of a Taylor cell spirals inwards and a particle that is initially close to the centre of the Taylor cell spirals outwards. The limit orbit is a single path which is contained in the darker region of Fig. 2(a). This banding is due to the path of each particle being close to its previous revolution as the limit orbit is approached. A large value of β has been used in this figure to more clearly illustrate the approach of the particle to its limit orbit. The rate at which the particle approaches its limit orbit is sensitive to the value of β. As β is decreased the particle path is more tightly packed resulting in a slower approach to the limit orbit. In Fig. 2(b) we plot contours of the stream function of the background flow together with the limit orbits of particles with density ratios $\beta = 1.01, 1.05, 1.1, 2, 5, 11$. On this scale the limit orbits for $1 < \beta \leqslant 2$ are indistinguishable from each other. Since the flow is steady, the stream function contours represent fluid element paths and we can see that the limit orbits of the particles do not correspond to fluid element paths. Relative to a fluid element path, the limit orbits are offset slightly, towards the inflow region of the Taylor cell, this effect is less pronounced as β is reduced.

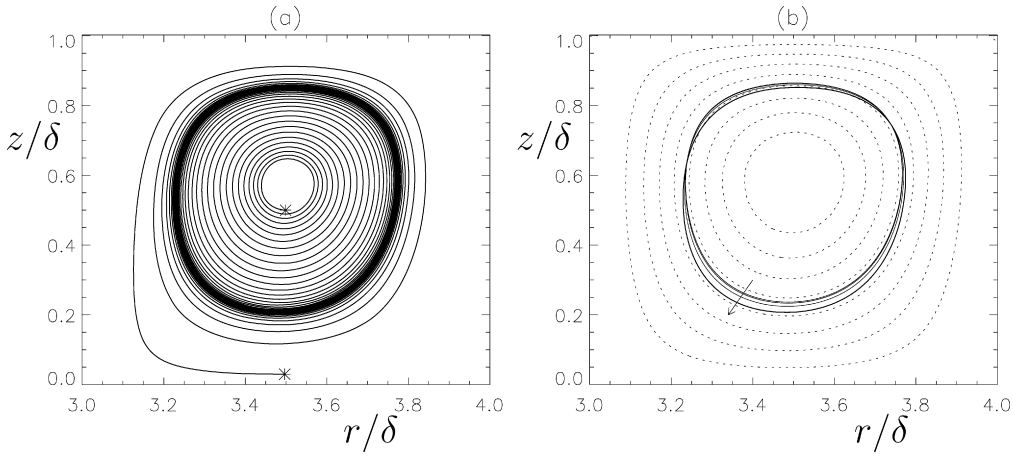

Fig. 2. (a) Paths of two particles ($\beta = 11$), whose initial positions are denoted by stars, in a background flow with Reynolds numbers $Re = 120$. The Taylor vortex is rotating clockwise. (b) Solid: Limit orbits for the particles with $\beta = 1.01, 1.05, 1.1, 2, 5, 11$, the arrow shows the direction of increasing β. Dotted: Contours of the stream function of the background flow. Each plot is over half a Taylor cell, with the inner rotating cylinder and the stationary outer cylinder located at $r/\delta = 3$, $r/\delta = 4$, respectively.

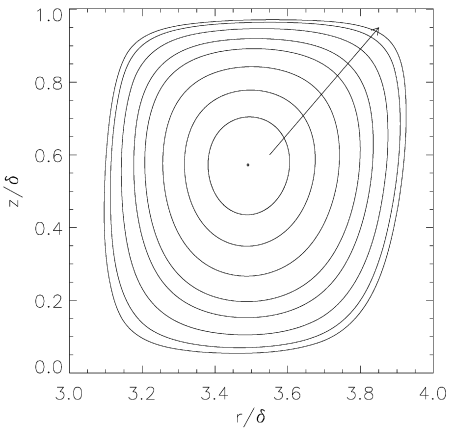

Fig. 3. Limit orbits for particles ($\beta = 1.05$) in a background flow at $Re = 100, 103, 107, 115, 130, 150, 200, 300, 400$. The arrow shows the direction of increasing Re.

In Fig. 3 we plot the limit orbits of particles for various Reynolds numbers. We find that for Reynolds numbers less than $Re^* \approx 100$, no visible limit orbit exists, instead all particles spiral towards the centre of the Taylor cell. Note that the critical Reynolds number at which Couette flow becomes unstable for this flow is $Re = 85.8$. As the Reynolds number is increased beyond Re^* we find that the limit orbit becomes larger.

The approach of the particles to the limit orbit is considered in Fig. 4. In Fig. 4(a) we plot the minimum distance, d, of the inner particle (as shown in Fig. 2(a)) from its limit orbit, as a function of time. This data is plotted as a solid line. As expected the general trend of d is to decrease with time but this occurs in a non-uniform way due to the different shape of the limit orbit compared to that of the particle path. This data may be *smoothed* to give $\bar{d}$ by averaging the values of d over the time, T, it takes for a particle to complete a revolution in the r–z plane. This data is plotted as a dashed line. The solid line in Fig. 4(b) is a plot of $\ln(\bar{d})$ against time. After an initial transient this data is approximately linear and we compute the line of best fit for the data shown, which is plotted as a dashed line parallel to the original data for clarity. Hence, after an initial transient, the convergence to the limit orbit is exponential and may be written as $\bar{d} = A\,\mathrm{e}^{-\kappa t}$. In Table 1 we give the values of the exponent, κ at various values of the Reynolds number for an inner and outer particle respectively. We denote a particle to be inner/outer if its initial position was inside/outside of the limit orbit. Given the domain of a Taylor cell to be $(r, z) \in [R_1, R_2] \times [0, \pi/k]$ we typically

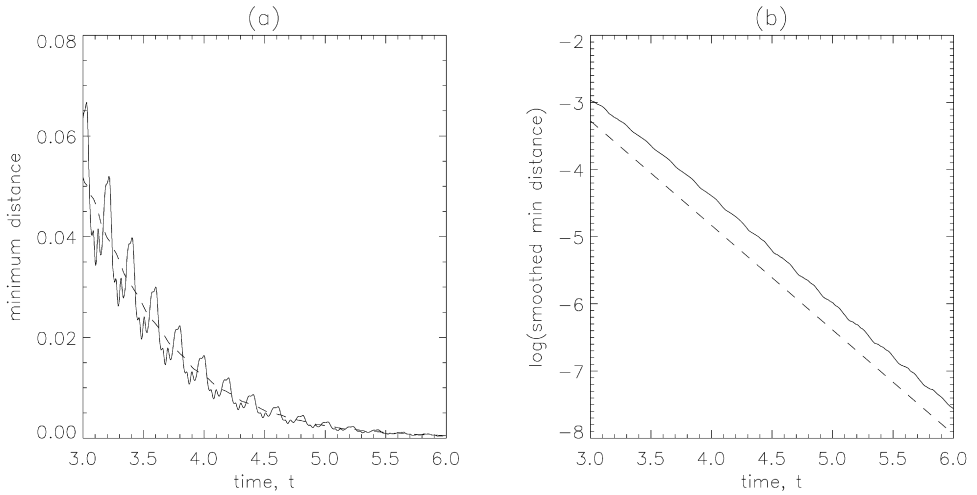

Fig. 4. (a) Solid: Plot of the minimum distance from the limit orbit against time for the inner particle ($\beta = 11$) in Fig. 2(a); Dashed: The smoothed minimum distance, $\bar{d}$, averaged over each revolution the particle makes in the r–z plane. (b) Plots of $\ln(\bar{d})$ for the data in Fig. 4(a). The dashed line represent the best straight line fit for the long-term behaviour of $\ln(\bar{d})$, shifted vertically for clarity.

Table 1
Values of the exponent κ for the inner and outer particles at various Reynolds numbers

Re	Exponent, κ	
	inner	outer
103	0.21	0.28
107	0.55	0.61
110	0.73	0.85
115	1.15	1.23
120	1.57	1.66
130	2.39	2.51
150	4.26	4.31

take the following initial values: $(r, z)_{\text{inner}} = (0.5(R_1 + R_2), 0.5\pi/k)$ and $(r, z)_{\text{outer}} = (0.5(R_1 + R_2), 0.05\pi/k)$. We see that at a fixed Reynolds number, the value of κ corresponding to the outer particle is always greater than that for the inner particle. Thus at sufficiently large time the outer particle will be closer to the inner particle than the inner particle. We can also see that the limit orbit is approached more rapidly as the Reynolds number increases. Note that it is not possible to get meaningful values for κ for $Re > 150$ as the limit orbit is reached so rapidly. For fixed α_p and β, over the range of values of Re shown, the exponent κ is approximately linear and by averaging κ over the inner and outer particle we find

$$\kappa \approx a(Re - b), \quad Re \geqslant 103,$$

where $a = 0.0858$, $b = 100.7$ in this case. We have investigated the dependence of a on the particle dimensions and have found that to leading order

$$a \propto (\beta - 1)/\alpha_p^2.$$

This dependence is illustrated in Fig. 5 in which we plot values of a against $(\beta - 1)/\alpha_p^2$ for several runs. Over the data points considered in Fig. 5 the value of b remains approximately constant. In general, the coefficients a and b will also be dependent on the radius ratio which in turn determines Re_c, the critical Reynolds number at which Couette flow becomes unstable.

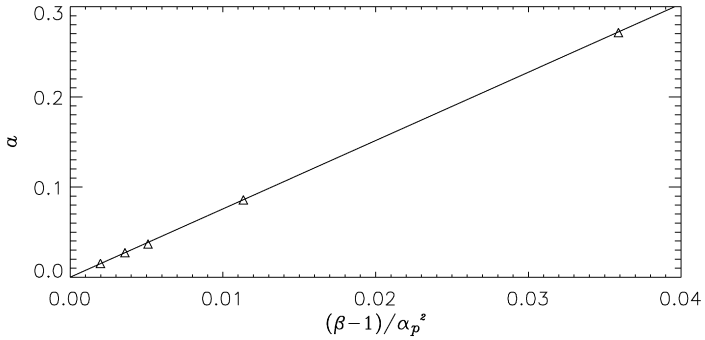

Fig. 5. Plot showing the linear dependence of a on the parameter $(\beta - 1)/\alpha_p^2$. The triangles represent numerical data.

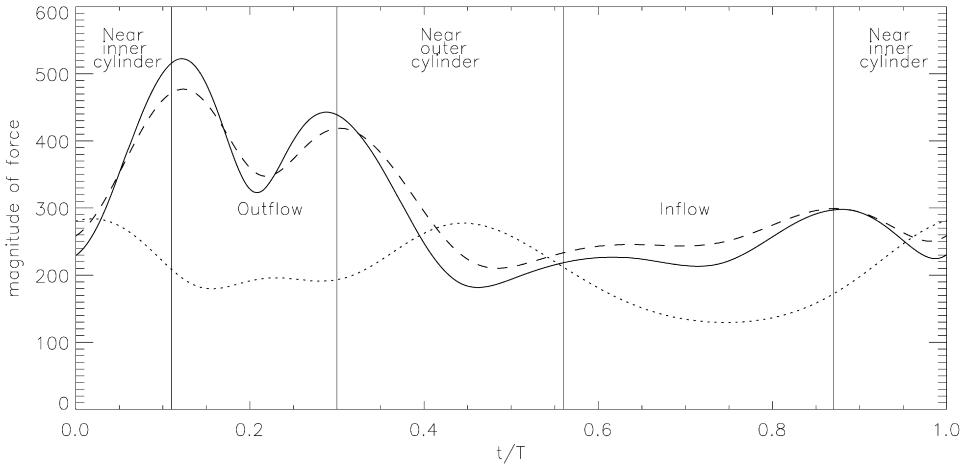

Fig. 6. The dimensionless magnitude of force in the (r, z) plane, over a complete limit orbit for a particle ($\beta = 1.05, \alpha = 29.6$) in a background flow with $Re = 120$. Solid: total force for the *control case* (neglecting Basset, Faxén and Saffman effects); Dashed: total force, including the Basset, Faxén and Saffman forces; Dotted: the combined Basset, Faxén and Saffman contributions.

3.2. Consideration of the forces acting on the particle

In Fig. 6 we consider the effect of including the Basset, Faxén and Saffman (BFS) forces on the total force acting on the particle in the (r, z) plane. The plot is over a complete cycle of the limit orbit in a flow with $Re = 120$. The plot is such that the particle is closest to the inner cylinder when $t/T = 0$ and $t/T = 1$ and closest to the outer cylinder when $t/T \approx 0.4$. The forces have been non-dimensionalised using length scale δ, viscous time scale δ^2/ν and mass scale m_p. The dashed line is a plot of the magnitude of the total force acting on the particle in the (r, z) plane for the computation in which Basset, Faxén and Saffman forces have been included. The BFS contribution to this total force is plotted as a dotted line.

It can be seen that the BFS contribution is of significant magnitude when compared to the magnitude of the total force. Hence one may expect the inclusion of these terms to have a pronounced effect on the particle. The magnitude of the total force acting on the particle in the (r, z) plane for the *control case* (neglecting Basset, Faxén and Saffman effects) is plotted as a solid line. We can see that the difference between the two plots for total force is much smaller than the contribution due to the BFS terms. This effect is also seen for each component (r, ϕ, z) but we present here the results for the magnitude only. We find that the contribution from the BFS terms is largely absorbed into the total force with compensatory changes occurring in the other contributory forces (drag, added mass, inertial, centrifugal and Coriolis). For example, considered individually, the Faxén term occurring in the drag force of Eq. (2) is of comparable order to the total BFS contribution. However, in including the Faxén term we find that, as a result of changes to the particle velocity, the difference in the total drag force between the control and the BFS case is an order of magnitude smaller than the corresponding Faxén contribution. It is clear that analysing the magnitudes of the Basset, Faxén and

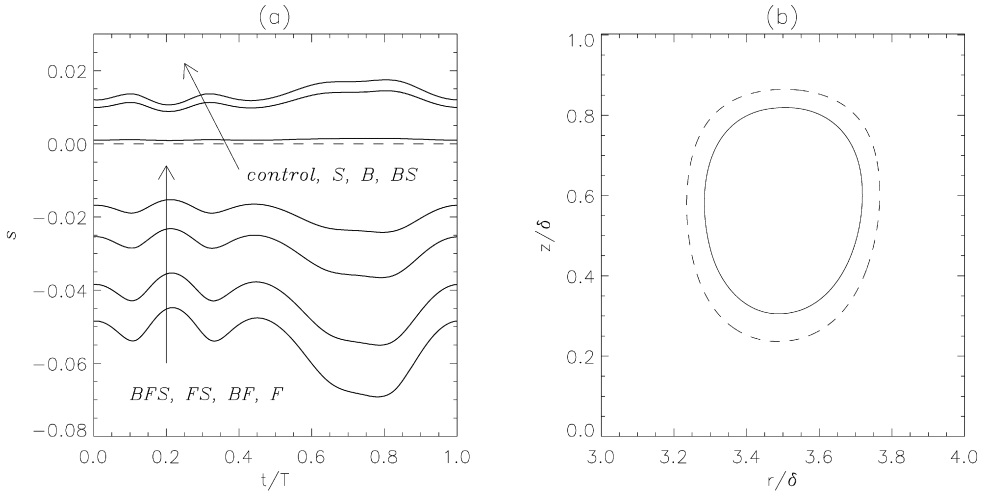

Fig. 7. Comparing the effect of including the Basset, Faxén and Saffman forces to the limit orbit of the *control case* of a particle ($\beta = 1.05$) in a flow with $Re = 120$. (a) Plots of the minimum distance, s, from the control limit orbit against time. The arrows and text indicate which forces have been included for each plot, where B, F, S represent Basset, Faxén and Saffman respectively. The dashed line represents the *control* case and negative values indicate that the limit orbit is within the limit orbit of the control case. (b) Limit orbits. Dashed: control case; Solid: including Basset, Faxén and Saffman (which gives the maximum deviation away from the control case).

Saffman terms in isolation may give misleading information as to the effects that these forces have on the eventual motion of a particle.

In Fig. 7(a) we consider in detail the effect of including the Basset (B), Faxén (F) and Saffman (S) forces on the limit orbit. All eight combinations of including/neglecting B, F and S are considered. The minimum distance, s, from the *control case* is plotted for each combination over a period of the orbit, where $t/T = 0$, 1 represents the time at which the particle is closest to the inner cylinder. Negative values indicate that the limit orbit is within that of the control case. Considered in isolation, the Faxén force reduces the size of the limit orbit, whilst the Basset and Saffman forces increase it. The effects from the Basset and Faxén forces are an order of magnitude greater than that due to Saffman.

In considering combinations of forces we see that in all the cases that include the Faxén force, a smaller limit orbit results compared to the control case. For such cases, the inclusion of either or both the B and S forces result in a further decrease in the size of the limit orbit compared to F alone. The effect is most pronounced when all three forces are included in the combination.

Non-linear effects are present; comparing the SF combination with the F case we see that the inclusion of the Saffman term reduces the size of the limit cycle further. This is in contrast to the effect of including Saffman alone. Similarly, the BF limit cycle is smaller than the F limit cycle despite the B limit cycle being larger than the control case. For the Basset case however, it should be noted that from Eq. (2) an extra term is present when a BF combination is considered. This term is absent when B or F are considered in isolation.

The limit cycle arising from the BFS case is plotted in Fig. 7(b) as a solid line together with the control case (dashed). We can see that, at this Reynolds number, there is a significant quantitative difference (approximately 20%) between the two limit orbits.

In Fig. 8 we investigate the effect of including the (a) Basset, (b) Faxén, (c) Saffman (d) all three terms (BFS) on the limit orbit, compared to the control case, for different Reynolds numbers and particle parameters. The quantity plotted in each case is, $\hat{s}$, the maximum of s/R over a complete period, where R represents the local radius of the control limit orbit. In this figure a dashed line represents a limit orbit within the control limit orbit and a solid line represents a limit orbit outside of the control limit orbit. From Fig. 8(a) we can see that the relative effect of including the Basset force is reduced as the Reynolds number of the background flow and the particle size ratio increases. However, changing the particle density has a negligible effect on the percentage deviation. From Fig. 8(b) we can see that the relative effect of including the Faxén corrections is reduced as the Reynolds number of the background flow increases. Changing the particle parameters has a pronounced effect. The maximum % deviation decreases with increasing $\alpha_p = \delta/2a_p$;

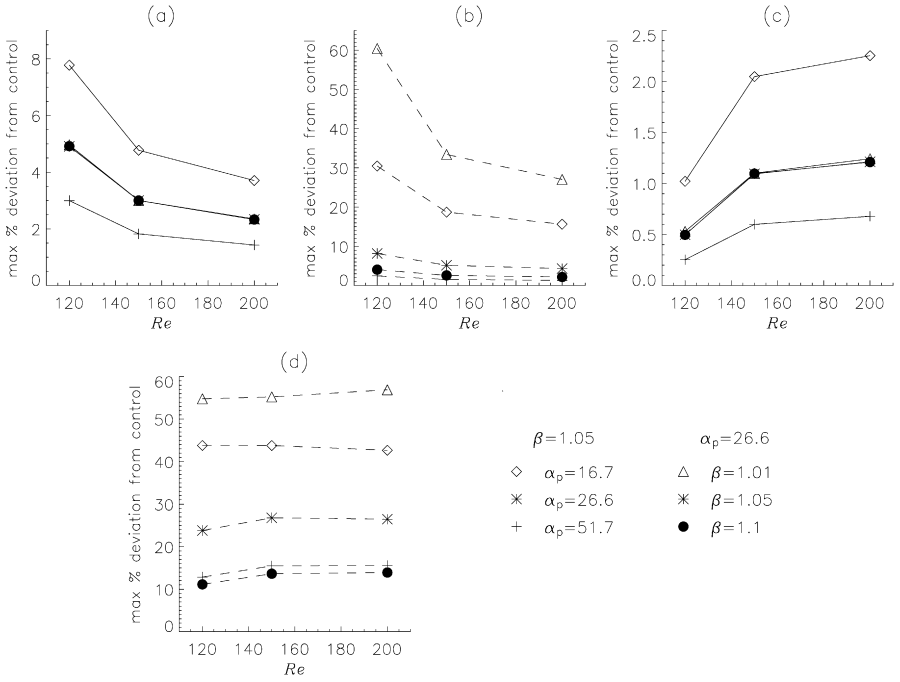

Fig. 8. Plots of $\hat{s} = \max(s/R)$, the maximum % deviation from the control limit orbit, against Reynolds number. Figs. (a) B, (b) F, (c) S, (d) BFS represent results for when the respective forces have been included in the calculation.

this is as expected given that the Faxén terms are proportional to a_p^2. There is also an increase in $\hat{s}$ as the density ratio approaches unity. From Fig. 8(c) we can see that the relative effect of including the Saffman force is increased as the Reynolds number of the background flow increases and as the particle ratio decreases. This behaviour is as expected given that the Saffman force is proportional to a_p^2. Changing the particle density has a negligible effect on the percentage deviation.

Including all three terms, as shown in Fig. 8(d), we see that the deviation from control is almost independent of the Reynolds number. This is in contrast to the cases in which the forces are considered in isolation. Both β and α_p have a significant effect on the limit cycle; the deviation from control is increased as the density ratio approaches unity and as the particle ratio decreases. Over the range of parameters shown the limit orbit is always totally within the control case. In general, the effect of including BFS is greater than the sum effect of the individual cases, as seen in Fig. 7(a).

4. Discussion

We have computed the path of a particle in a Taylor vortex and have found that it tends to a limit orbit in the meridional plane. The key aims of this paper were firstly to investigate the effect that increasing the Reynolds number of the background flow has on the subsequent path of the particle. The second aim was to analyse the effects that the Basset, Faxén and Saffman forces have on the particles' resulting motion.

By using a numerical solution of the Navier–Stokes equations to describe the background flow we have been able to explore a wider range of Reynolds numbers than those considered by Wereley and Lueptow [17]. We show that the limit orbit that they discovered (at 23% above Re_c) occurs also at much higher Reynolds numbers. We find that as the Reynolds number of the background flow increases, the size of the limit orbit of the particle also increases. We show that the approach to the limit orbit occurs more rapidly at higher Reynolds numbers. After an initial transient, the approach to the limit orbit is exponential where the exponent is proportional to $(\beta - 1)Re/\alpha_p^2$. For a given set of fluid and particle parameters, this relationship could be used to estimate the *settling time*, the average time taken for a particle to be a certain distance from the limit orbit. This could be used by experimentalists depending on whether the goal is to visualise paths close to fluid element paths or to limit orbit cycles.

We have also considered the effects that the Basset (B), Faxén (F) and Saffman (S) forces have on the particles' resulting motion. We note that the sometimes large magnitudes of the B, F and S forces do not result in a corresponding large effect on the total force. Hence, analysing the magnitude of these forces alone, will not necessarily give a quantitative indication of the effect BFS terms on the limit orbit. We find that, considered in isolation, the inclusion of B or S increases the size of the limit orbit, whilst F decreases it. However when all three forces are considered together the limit orbit is always within that of the control and, for nearly all parameter values considered, represents the combination that gives the greatest deviation. This deviation does not depend strongly on the Reynolds number, but increases dramatically as $\beta \to 1$ and as α_p decreases. For the results presented in Fig. 8(d) we find the deviation varies from 11% to 57% and conclude that all three forces must be included in the calculation to accurately predict the limit orbit. It should be noted however that when the B, F and S terms are considered we only present results for the limit orbits as opposed to the approach to the limit orbits. We anticipate, from the relationship observed in Fig. 5, that as β approaches unity, the settling time will increase, hence the relatively large differences that we find between the limit orbits of the control and BFS cases may only be evident after a long time period.

One of the motivations for this paper is the recent developments in using PIV in helium II [28,4–6]. Helium II is the phase of liquid helium that exists between absolute zero and the transition temperature of $T_\lambda = 2.1768$ K and can be well described (according to Landau's two-fluid theory) to be made up of two completely mixed components: the viscous normal fluid and the inviscid superfluid. At temperatures higher than T_λ liquid helium is called helium I and is an ordinary viscous fluid which obeys the classical Navier–Stokes equations. We thus expect that tracer particles in helium II are subject to inertial forces which arise from both the normal fluid and the superfluid, and to viscous forces which arise from the normal fluid alone. Since the relative proportion of normal fluid and superfluid is a strong function of temperature, which can be changed very easily in the experiments, the relative proportion of these forces can vary greatly. Similarly, a small increase of temperature can turn helium II into ordinary helium I. Now the Taylor–Couette problem of helium II has received considerable attention over the years [29–32,7] and has become a benchmark problem of low temperature fluid dynamics. In particular, it was used with success to test the two-fluids equations of motion of helium II. Couette flow is thus a natural benchmark to test the equations of motion of small particles in two-fluid hydrodynamics which have been proposed recently [33]. It is therefore important to have a good understanding of the motion of particles in the ordinary Couette problem (helium I) and the relative importance of the various forces, which is what we set out to do in this work.

Acknowledgements

CFB is grateful to EPSRC for supporting this research. We would like to thank Professor Yuri Sergeev for his interest in this work and his useful comments.

References

[1] M.R. Maxey, J.J. Riley, Equation of motion for a small rigid sphere in a nonuniform flow, Physics of Fluids 26 (1983) 883–889.
[2] T.R. Auton, J.C.R. Hunt, M. Prud'homme, The force exerted on a body in inviscid unsteady non-uniform rotational flow, Journal of Fluid Mechanics 197 (1988) 241–257.
[3] R.W. Mei, Flow due to an oscillating sphere and an expression for unsteady drag on the sphere at finite Reynolds number, Journal of Fluid Mechanics 270 (1994) 133–174.
[4] T. Zhang, D. Celik, S.W. Van Sciver, Tracer particles for application to PIV studies of liquid helium, Journal of Low Temperature Physics 134 (2004) 985–1000.
[5] T. Zhang, S.W. Van Sciver, Large-scale turbulent flow around a cylinder in counterflow superfluid 4He, Nature Physics 1 (2005) 36–38.
[6] G.P. Bewley, D.P. Lathrop, K.R. Sreenivasan, Visualization of quantized vortices, Nature 441 (2006) 588.
[7] K.L. Henderson, C.F. Barenghi, C.A. Jones, Nonlinear Taylor–Couette flow of helium II, Journal of Fluid Mechanics 283 (1995) 329–340.
[8] P.K. Dutta, A.K. Ray, Experimental investigation of Taylor vortex photocatalytic reactor for water purification, Chemical Engineering Science 59 (2004) 5249–5259.
[9] B. Haut, H. Ben Amor, L. Coulon, A. Jacquet, V. Halloin, Hydrodynamics and mass transfer in a Couette–Taylor bioreactor for the culture of animal cells, Chemical Engineering Science 58 (2003) 777–784.
[10] A. Babiano, J.H.E. Cartwright, O. Piro, A. Provenzale, Dynamics of a small neutrally buoyant sphere in a fluid and targeting in Hamiltonian systems, Physical Review Letters 84 (2000) 5764–5767.
[11] E.E. Michaelides, Review – The transient equation of motion for particles, bubbles and droplets, Journal of Fluids Engineering 119 (1997) 233–247.
[12] R.M. Lueptow, Fluid mechanics of a rotating filter separator, in: K.J. Choi (Ed.), Advances in Filtration and Separation Technology, vol. 9, American Filtration and Separations Society, 1995, pp. 283–291.

[13] U.B. Holeschovsky, C.L. Cooney, Quantitative description of a ultrafiltration in a rotating filtration device, AIChE Journal 37 (1991) 1219–1226.
[14] G. Belfort, P. Mikulasek, J.M. Pimbley, K.Y. Chung, Diagnosis of membrane fouling using a rotating annular filter. 2. Dilute particle suspensions of known particle-size, Journal of Membrane Science 77 (1993) 23–39.
[15] M. Rudman, Particle shear-rate history in a Taylor–Couette column, Liquid–solid flows, ASME 189 (1994) 23–30.
[16] M. Rudman, Mixing and particle dispersion in the wavy vortex regime of Taylor–Couette flow, AIChE Journal 44 (1998) 1015–1026.
[17] S.T. Wereley, R.M. Lueptow, Velocity field for Taylor–Couette flow with an axial flow, Physics of Fluids 11 (1999) 325–333.
[18] A. Davey, The growth of Taylor vortices in flow between rotating cylinders, Journal of Fluid Mechanics 14 (1962) 336–368.
[19] K.L. Henderson, C.F. Barenghi, Numerical methods for helium's two fluid model, Journal of Low Temperature Physics 98 (1995) 351–381.
[20] A.B. Basset, On the motion of a sphere in a viscous liquid, Philosophical Transactions of the Royal Society of London 179 (1888) 43–63.
[21] R. Mei, R.J. Adrian, Flow past a sphere with an oscillation in the free-stream velocity and unsteady drag at finite Reynolds number, Journal of Fluid Mechanics 237 (1992) 323–341.
[22] E.E. Michaelides, A novel way of computing the Basset term in unsteady multiphase flow computations, Physics of Fluids A 4 (1992) 1579–1582.
[23] F. Candelier, J.R. Angilella, M. Souhar, On the effect of the Boussinesq–Basset force on the radial migration of a Stokes particle in a vortex, Physics of Fluids 16 (2004) 1765–1776.
[24] M.W. Reeks, S. McKee, The dispersive effects of Basset history forces on particle motion in a turbulent flow, Physics of Fluids 27 (1984) 1573–1582.
[25] P.J. Thomas, On the influence of the Basset history force on the motion of a particle through a fluid, Physics of Fluids A 4 (1992) 2090–2093.
[26] C.M. Coimbra, M.H. Kobayashi, On the viscous motion of a small particle in a rotating cylinder, Journal of Fluid Mechanics 469 (2002) 257–286.
[27] Y. Murai, H. Oiwa, Y. Taked, Bubble behavior in a vertical Taylor–Couette flow, Journal of Physics: Conference Series 14 (2005) 143–156.
[28] R.J. Donnelly, A.N. Karpetis, J.J. Niemela, K.R. Sreenivasan, W.F. Vinen, C.M. White, The use of particle image velocimetry in the study of turbulence in liquid helium, Journal of Low Temperature Physics 126 (2002) 327–332.
[29] S. Chandrasekhar, R.J. Donnelly, The hydrodynamic stability of He II between rotating cylinders. I, Proceedings of the Royal Society of London A 241 (1957) 9–28.
[30] C.F. Barenghi, C.A. Jones, The stability of the Couette flow of helium II, Journal of Fluid Mechanics 197 (1988) 551–569.
[31] C.J. Swanson, R.J. Donnelly, Instability of Taylor–Couette flow of helium II, Physical Review Letters 67 (1991) 1578–1581.
[32] C.F. Barenghi, Vortices and the Couette flow of helium II, Physical Review B 45 (1992) 2290–2293.
[33] D.R. Poole, C.F. Barenghi, Y.A. Sergeev, W.F. Vinen, Motion of tracer particles in He II, Physical Review B 71 (2005) 064514.